Article

Interchain-expanded extra-large-pore zeolites

https://doi.org/10.1038/s41586-024-07194-6

Received: 30 March 2023

Accepted: 12 February 2024

Published online: 27 March 2024

Check for updates

Zihao Rei Gao[1,15,16], Huajian Yu[1,16], Fei-Jian Chen[2,16], Alvaro Mayoral[3], Zijian Niu[2], Ziwen Niu[4], Xintong Li[4], Hua Deng[5], Carlos Márquez-Álvarez[6], Hong He[5,7], Shutao Xu[8], Yida Zhou[8], Jun Xu[9], Hao Xu[4], Wei Fan[10], Salvador R. G. Balestra[1,11], Chao Ma[12], Jiazheng Hao[13,14], Jian Li[12]✉, Peng Wu[4]✉, Jihong Yu[2]✉ & Miguel A. Camblor[1]✉

Stable aluminosilicate zeolites with extra-large pores that are open through rings of more than 12 tetrahedra could be used to process molecules larger than those currently manageable in zeolite materials. However, until very recently[1–3], they proved elusive. In analogy to the interlayer expansion of layered zeolite precursors[4,5], we report a strategy that yields thermally and hydrothermally stable silicates by expansion of a one-dimensional silicate chain with an intercalated silylating agent that separates and connects the chains. As a result, zeolites with extra-large pores delimited by 20, 16 and 16 Si tetrahedra along the three crystallographic directions are obtained. The as-made interchain-expanded zeolite contains dangling Si–CH_3 groups that, by calcination, connect to each other, resulting in a true, fully connected (except possible defects) three-dimensional zeolite framework with a very low density. Additionally, it features triple four-ring units not seen before in any type of zeolite. The silicate expansion–condensation approach we report may be amenable to further extra-large-pore zeolite formation. Ti can be introduced in this zeolite, leading to a catalyst that is active in liquid-phase alkene oxidations involving bulky molecules, which shows promise in the industrially relevant clean production of propylene oxide using cumene hydroperoxide as an oxidant.

Very recently, we reported a case of a one-dimensional to three-dimensional (1D to 3D) topotactic condensation of a complex chain silicate zeolite precursor (ZEO-2) into the extra-large-pore ZEO-3 zeolite[2]. ZEO-3 has a 3D system of pores open through rings containing 16, 14 and 14 tetrahedra. Here we intercalated Si atoms between the chains (Fig. 1). The interchain-expanded reaction produced new zeolite structures, which were solved and refined by combining state-of-the-art 3D electron diffraction and synchrotron powder X-ray diffraction data (SPXRD). The reactions that introduce silicon between the chains of ZEO-2 (Fig. 1a) are carried out in acidic ethanolic solution using either dimethyldichlorosilane (DCDMS; containing a single Si per molecule) or 2,4,6,8-tetramethylcyclotetrasiloxane (TMCTS; a single four-ring (*s4r*) containing four Si per molecule with methyl and H substituents at each Si corner). The reaction results in the intercalation of new silicon atoms in between adjacent chains, connecting them together in a new stable crystalline zeolite (powder X-ray diffraction data are shown in Fig. 2f). Depending upon whether the silylating agent used was DCDMS or TMCTS, the material ZEO-4A (Fig. 1b) or ZEO-4B (Fig. 1c), respectively, was produced. Both retain the needle-like morphology of ZEO-2 (Extended Data Fig. 1)[2]. Discrete double four-ring silica units (*d4r*) have been connected before with silylating agents but resulted in complex non-crystalline silicone copolymers[6]. The materials reported in this work were developed in the Instituto de Ciencia de Materiales de Madrid, Consejo Superior de Investigaciones Científicas, Spain, but the ZEO nomenclature following the previous ZEO-1 to ZEO-3 has been used for convenience.

In view of the synthesis procedure used and the magic angle spinning (MAS) nuclear magnetic resonance (NMR) results shown in Fig. 2d, it was possible for us to model the structures of ZEO-4A and ZEO-4B. These were then optimized using density functional tight binding methods (details are in Supplementary Information). Nonetheless, the structures of ZEO-4A and ZEO-4B were also solved ab initio from

[1]Instituto de Ciencia de Materiales de Madrid (ICMM), CSIC, Madrid, Spain. [2]State Key Laboratory of Inorganic Synthesis and Preparative Chemistry, College of Chemistry, International Center of Future Science, Jilin University, Changchun, China. [3]Instituto de Nanociencia y Materiales de Aragón (INMA), CSIC–Universidad de Zaragoza, Zaragoza, Spain. [4]Shanghai Key Laboratory of Green Chemistry and Chemical Processes, School of Chemistry and Molecular Engineering, East China Normal University, Shanghai, China. [5]Center for Excellence in Regional Atmospheric Environment, Key Laboratory of Urban Pollutant Conversion, Institute of Urban Environment, Chinese Academy of Sciences, Xiamen, China. [6]Instituto de Catálisis y Petroleoquímica (ICP), CSIC, Madrid, Spain. [7]State Key Joint Laboratory of Environment Simulation and Pollution Control, Research Center for Eco-Environmental Sciences, Chinese Academy of Sciences, Beijing, China. [8]National Engineering Research Center of Lower-Carbon Catalysis Technology, Dalian Institute of Chemical Physics, Chinese Academy of Sciences, Dalian, China. [9]National Center for Magnetic Resonance in Wuhan, State Key Laboratory of Magnetic Resonance and Atomic and Molecular Physics, Wuhan Institute of Physics and Mathematics, Innovation Academy for Precision Measurement Science and Technology, Chinese Academy of Sciences, Wuhan, China. [10]Department of Chemical Engineering, University of Massachusetts, Amherst, MA, USA. [11]Departamento de Sistemas Físicos, Químicos y Naturales, Universidad Pablo de Olavide, Seville, Spain. [12]State Key Laboratory of Coordination Chemistry, School of Chemistry and Chemical Engineering, Nanjing University, Nanjing, China. [13]Spallation Neutron Source Science Center, Dongguan, China. [14]Institute of High Energy Physics, Chinese Academy of Sciences, Beijing, China. [15]Present address: Department of Chemical and Biomolecular Engineering and Institute for NanoBioTechnology, Johns Hopkins University, Baltimore, MD, USA. [16]These authors contributed equally: Zihao Rei Gao, Huajian Yu, Fei-Jian Chen. ✉e-mail: jian.li@nju.edu.cn; pwu@chem.ecnu.edu.cn; jihong@jlu.edu.cn; macamblor@icmm.csic.es

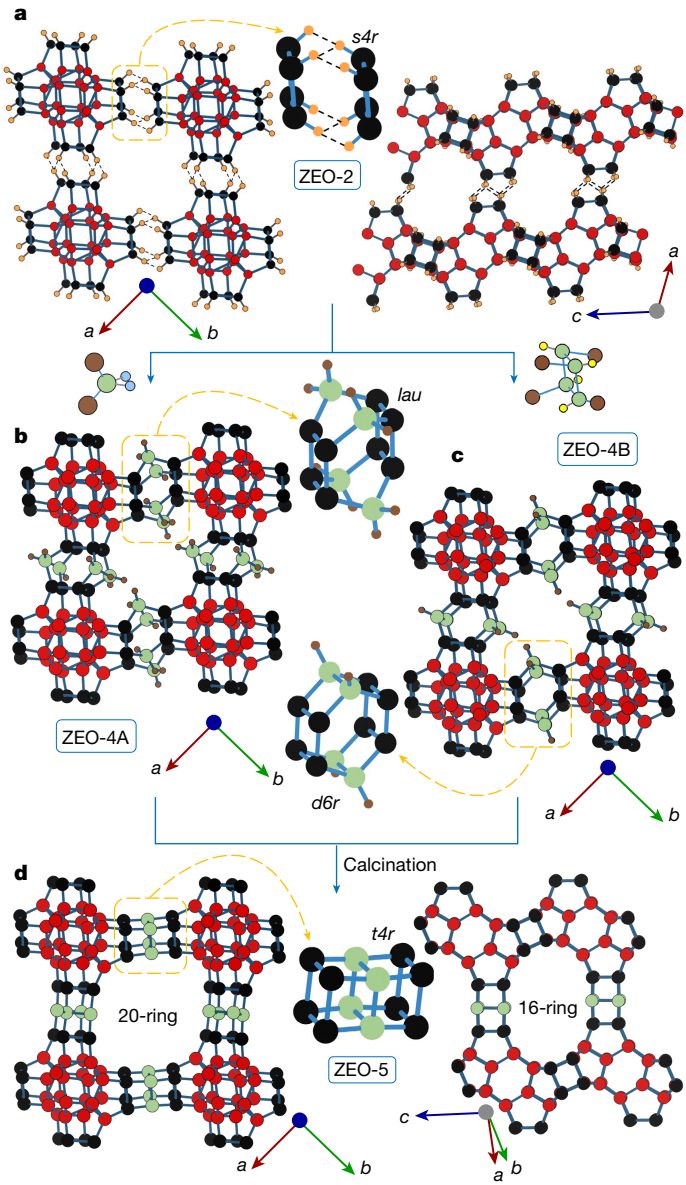

Fig. 1 | Preparation and structure of ZEO-4A, ZEO-4B and ZEO-5. **a**–**d**, Silylation of ZEO-2 (**a**) produces the interchain-expanded zeolites ZEO-4A (**b**) and ZEO-4B (**c**), two interrupted zeolites that, upon calcination, yield the same non-interrupted zeolite, ZEO-5, containing a 3D system of extra-large 20 × 16 × 16 ring pores (**d**). Relevant structural units are highlighted in orange dashed rectangles; the starting hydrogen-bonded *s4r* (**a**) is connected by D^2 Si atoms forming *lau* units in ZEO-4A (**b**) or T^3 Si atoms forming double six-ring units, *d6r*, in ZEO-4B (**c**), which are fully connected by calcination into a new *t4r* (**d**) where all the atoms are Q^4. Bridging O atoms are omitted for clarity. Methyl groups are brown, chloride is light blue and hydrogen directly bonded to Si is yellow. Si atoms are distinguished by colour as Si that remains Q^4 during the whole process from **a** to **d** (red), Si that is Q^3 before the interchain expansion (black) and Si introduced during the interchain expansion reaction (green). All the Si atoms in **d** are Q^4.

continuous rotation electron diffraction (cRED) data (Supplementary Figs. 1 and 2 and Supplementary Tables 1, 2 and 5). The positions of silicon and oxygen atoms in the framework structures could be located directly in the observed electrostatic potential maps (Supplementary Fig. 3). The positions of some dangling Si–CH_3 groups were derived from a difference potential map during the course of the refinement (Supplementary Fig. 4). The resulting ZEO-4 materials contain nominally extra-large 20 × 16 × 16 ring pores and present two structurally different variants of the interchain-expanded interrupted zeolite because of the different silylating agents used. The DCDMS silylating agent in ZEO-4A contains two methyl groups per Si and connects two ZEO-2 silica chains by oxygen bridges (four per four-ring of the chains) while retaining both methyl groups. In ZEO-4B, on the other hand, TMCTS has only a single methyl group per Si and connects ZEO-2 chains through SiOSi pairs (two per four-ring). The final configuration of the newly introduced Si in ZEO-4B implies the breaking of the TMCTS ring in the acid alcohol solution. In both ZEO-4 materials, the dangling Si–CH_3 groups should effectively reduce the pore apertures and provide a four-lobed shape of the windows along [001], reducing the effective entrance (Extended Data Fig. 2). To obtain more accurate atomic positions, the structures of ZEO-4A and ZEO-4B, including the position of the dangling Si–CH_3 groups, were refined against SPXRD using the Rietveld method (Extended Data Fig. 3 and Supplementary Tables 7–11).

The ^{29}Si MAS NMR spectra of ZEO-4A and ZEO-4B demonstrate the insertion of the silylating agents in both materials, as they show either D^2 (that is, $Si(OSi)_2(CH_3)_2$ at −16 and −13 ppm) or T^3 (that is, $Si(OSi)_3(CH_3)$ at −65 and −63 ppm) resonances, respectively (Fig. 2d). The reason for the double resonances is that the silanes exist in two different crystallographic sites in both materials. All remaining resonances are assigned to Q^4 species (that is, $Si(OSi)_4$ in the range of −108 to −114 ppm), indicating that the originally abundant Q^3 (that is, $Si(OSi)_3OH$ or $Si(OSi)_3O^-$) species in ZEO-2 (ref. 2) have essentially all been connected to the newly inserted Si. These structures have been confirmed by ^{1}H–^{29}Si heteronuclear correlation experiments on ZEO-4A and ZEO-4B (Supplementary Figs. 16 and 17). Additionally, ^{13}C MAS NMR shows mainly resonances assigned to the methyl groups at −3 and −8 ppm for ZEO-4A and ZEO-4B (Supplementary Fig. 12a), respectively. Furthermore, no ^{31}P MAS NMR signal is detected in ZEO-4A or ZEO-4B (Supplementary Fig. 12b), showing that all the organic structure-directing agent (OSDA) in the starting ZEO-2 material has been removed from the zeolite during the reaction. This is corroborated by the ^{13}C and ^{31}P liquid NMR of the filtrate solution (Supplementary Fig. 10), which shows that the OSDA can be recovered intact. Self-supported Fourier transform infrared spectra on ZEO-4 are also consistent with the silylation and OSDA removal during the procedure (Supplementary Fig. 11).

Preparation and structure of ZEO-5

Calcination of both variants of ZEO-4 removes the methyl groups from the silylating agents and condenses adjacent Si–OH groups to produce a full connectivity of the newly introduced Si atoms and thereby, the new zeolite ZEO-5 (Fig. 1d). Accordingly, the ^{29}Si MAS NMR spectra (Fig. 2d) contain only Q^4 silicon resonances and are essentially identical irrespective of the starting material, apart from minor differences in peak broadening and resolution. The small concentration of Q^3 resonances is demonstrated by the poor-intensity enhancement under ^{29}Si{^{1}H} cross-polarization conditions. A resonance at −98.6 ppm in the direct irradiation spectra, which is not enhanced under cross-polarization, is at an unusually low field for a Q^4 Si site in SiO_2 zeolites (at least 6 ppm at a lower field than previous reports), but we attribute this to the very sharp Si–O–Si angles at the responsible Si site. Contrarily to ZEO-5, interlayer expanded zeolites are interrupted frameworks rather than true zeolites because dangling Si–R or Si–OH groups are structurally required in the final as-made and calcined materials, respectively[7,8].

The single-crystal structure of ZEO-5 was solved ab initio by using cRED (Fig. 2c). The cRED data were collected on the calcined crystals of both variants of ZEO-4 separately, and both resulted in *C*-centred monoclinic symmetry with a resolution of approximately 0.80 Å and more than 95% completeness (Supplementary Figs. 5 and 6 and Supplementary Tables 3, 4 and 6). The structures of calcined ZEO-5A and ZEO-5B were solved directly in space group *C*2/*c*, with all silicon and oxygen atoms directly located from the observed difference potential maps, and are identical. The structure contains two fused double

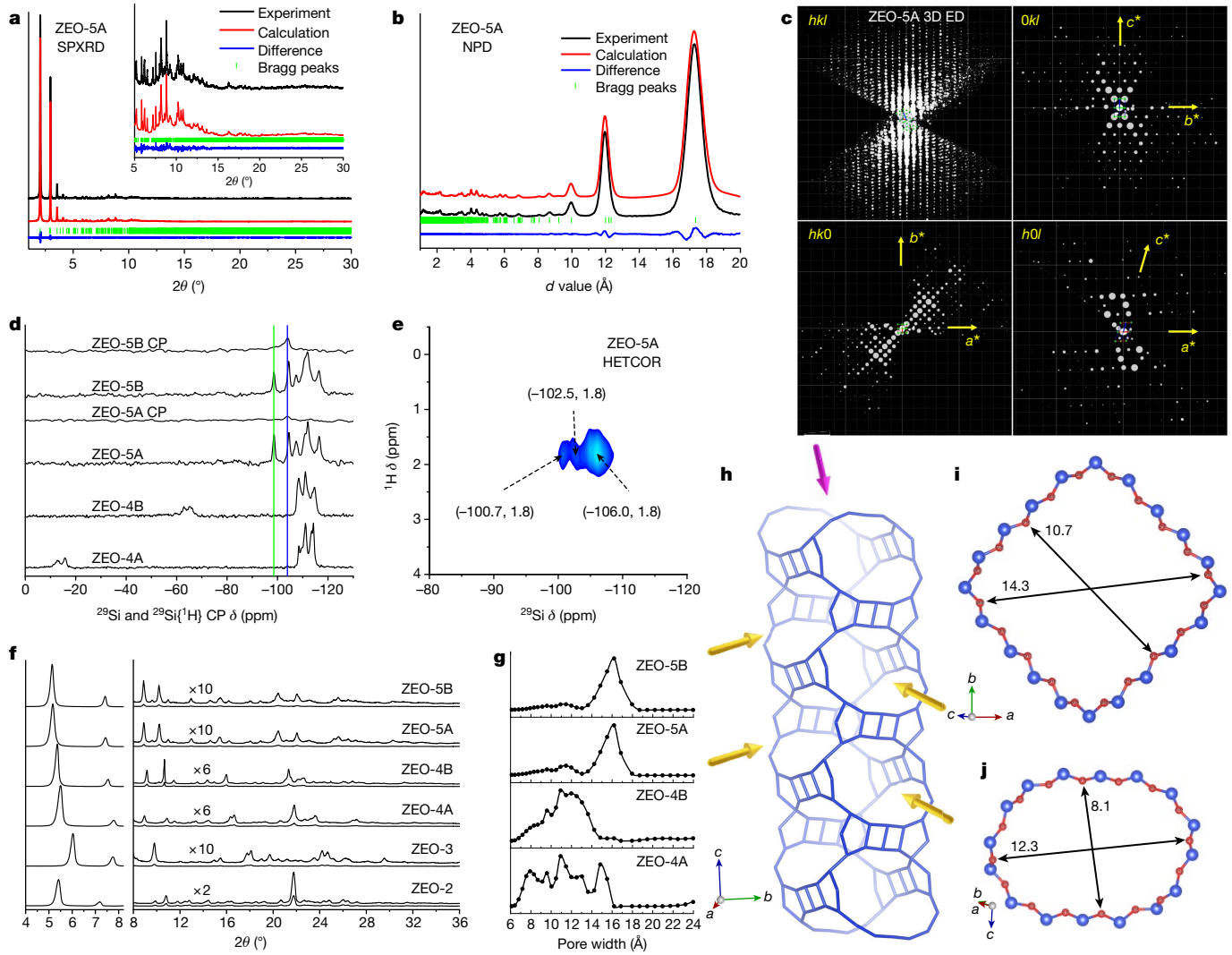

Fig. 2 | Characterization of ZEO-4 and ZEO-5. a–**c**, SPXRD (**a**, with the high-angle range shown in the inset) and NPD (**b**) Rietveld plots of ZEO-5A refined combining 3D electron diffraction, SPXRD and NPD data, and projection of the 3D reciprocal lattice reconstructed from a typical cRED dataset (**c**). **d**, ^{29}Si MAS NMR spectra. ZEO-4 materials contain either D^2 or T^3 atoms in addition to Q^4 but not a notable concentration of Q^3. ZEO-5 contains mainly Q^4, and just a minor concentration of Q^3 connectivity defects at around −104 ppm, highlighted by the blue vertical line. The green vertical line highlights a low-field Q^4 resonance around −98 ppm. **e**, ^{1}H–^{29}Si heteronuclear correlation (HETCOR) MAS NMR spectra showing no enhancement of the −98 ppm resonance, confirming the conclusion from **d**; spectra are recorded with 1.5 ms contact time (other contact time spectra are shown in Supplementary Fig. 21). **f**, Laboratory powder X-ray diffraction data patterns: ZEO-2, ZEO-3, ZEO-4A, ZEO-4B, ZEO-5A and ZEO-5B are shown from bottom to top. **g**, Pore size distributions of ZEO-4 and ZEO-5 calculated by the non-localized density functional theory (NLDFT) method from argon adsorption isotherms (Supplementary Fig. 8). **h**, The 3D channel system in ZEO-5. The saddle-shaped 20-ring channels (purple arrow) of ZEO-5 are crossed by the 16-ring channels (yellow arrows). **i**,**j**, Crystallographic clearance of 20- (**i**) and 16-ring (**j**) pores in ångströms. The arrows show the longest and shortest distances; the van der Waals radius of O (2 × 1.35 Å) has been subtracted. CP, cross-polarization.

four-ring units that we call triple four-ring (*t4r*), which has never been seen before in a zeolite, either natural or synthetic, regardless of the chemical composition. The existence of *t4r* units in ZEO-5 was double checked by removing the central four-ring from the structural model and examining the difference potential map using high-quality cRED data (Supplementary Fig. 7). The framework of ZEO-5 was refined anisotropically against the cRED data, and the refinement converged to unweighted residual factor (R_1) values of 0.1191 and 0.1268 for the material obtained from ZEO-4A and ZEO-4B, respectively (Supplementary Table 6). Further refinement by the Rietveld method of the structure of ZEO-5 against combined cRED, SPXRD and neutron powder diffraction (NPD) datasets was performed to obtain more precise bond lengths and angles (Fig. 2a,b and Supplementary Tables 12–15). The three types of diffraction data were simultaneously used for structural refinement, and the same set of crystallographic parameters (the atomic coordinate parameters, anisotropic displacement factors, unit cell parameters, occupancy) was shared and opened to refine without geometry restraints. Most Si–O–Si and O–Si–O angles are consistent with conventional understanding of zeolites, but four Si–O–Si and two O–Si–O angles in the *t4r* are unusual, which we consider related to the unusually low-field Q^4 resonance in ZEO-5. With the precise structural model in hand, we assign the −98.6 ppm resonance mentioned to the Si atoms in the central four-ring of the *t4r* (Si12 and Si13 with average Si–O–Si angles in the Rietveld refined structure of 137.1° and 137.0°, respectively). Using the correlation from ref. 9 and the distances and angles from our combined refinement, the calculated chemical shifts for ZEO-5 fall in two well-separated ranges: −103 to −117 ppm for the 'unstrained' sites Si1 to Si11 and −94 to −97 ppm for the 'strained' Si12 and Si13. Additionally, we have optimized ZEO-5 by density functional theory and calculated the ^{29}Si chemical shift of each individual Si site

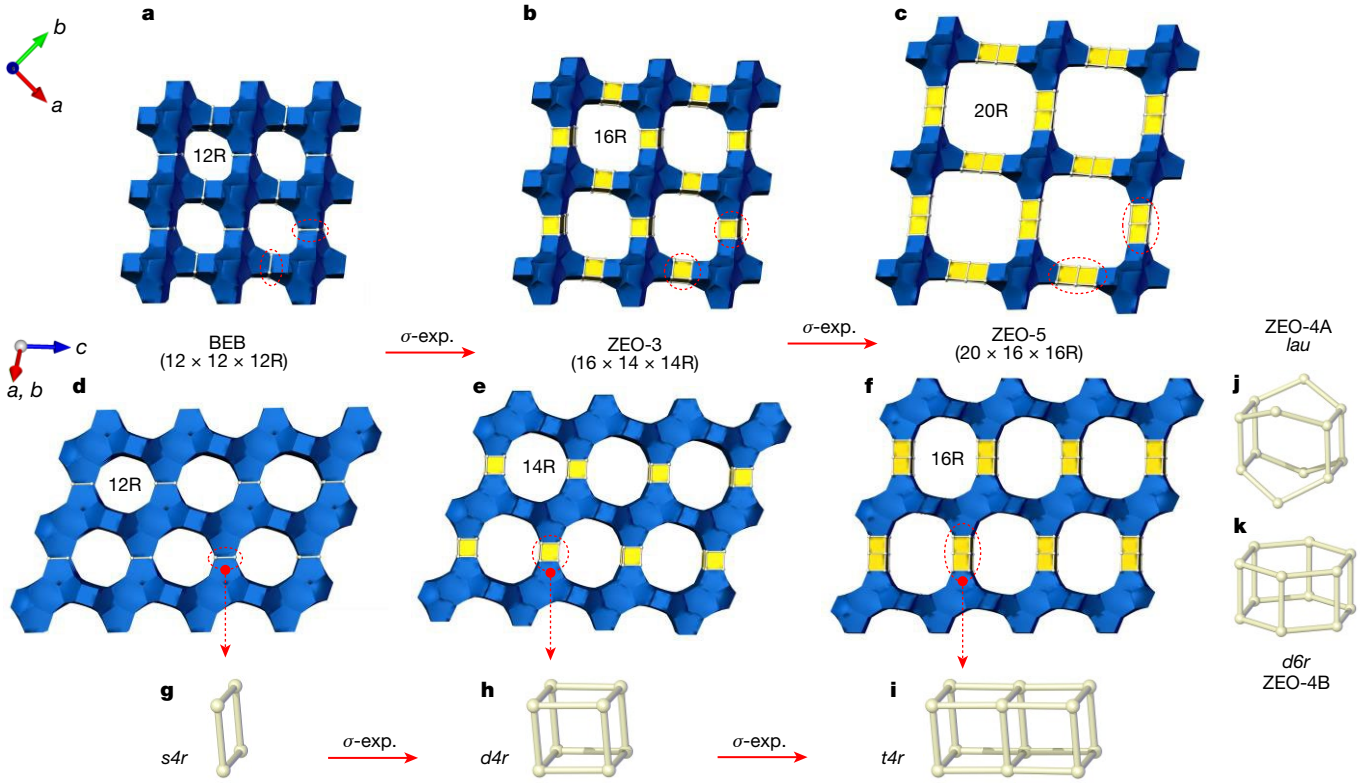

Fig. 3 | Generation of extra-large pores by *σ*-expansion. a–**i**, A *σ*-expansion (*σ*-exp.) of polymorph B of the 3D large-pore zeolite Beta (here denoted as BEB) (**a**,**d**) converts an *s4r* (**g**) into *d4r* (**h**) and generates the 3D extra-large-pore ZEO-3 (**b**,**e**), whereas a *σ*-exp. of ZEO-3 converts a *d4r* into a *t4r* (**i**) and generates ZEO-5 (**c**,**f**), with even larger pores. Panels **a**–**c** are views along [001] and **d**–**f** are along [1$\bar{1}$0]. **j**,**k**, The *t4r* is derived from the *lau* unit in ZEO-4A (**j**) or the *d6r* in ZEO-4B (**k**). The first of the *σ*-exp. mentioned (BEB to ZEO-3) is merely hypothetical, whereas the second one (ZEO-3 to ZEO-5) has some real meaning because ZEO-5 is made by the actual insertion of four Si atoms between the chains of the ZEO-3 precursor ZEO-2.

obtaining a good correspondence with the experimental results and supporting the assignation of the −98.6 ppm resonance (calculated −96.8 ppm) to the Si in the central four-ring of the *t4r* (Extended Data Fig. 4). The structural models derived by cRED and Rietveld refinement have been confirmed by spherical aberration-corrected (Cs-corrected) scanning transmission electron microscopy (STEM) imaging (Extended Data Fig. 5). Spectra from ^{1}H MAS NMR (Supplementary Fig. 18) and ^{1}H double-quantum/single-quantum MAS NMR (Supplementary Fig. 19) indicate predominance of weakly hydrogen bonded silanols at 1.8 ppm.

ZEO-5 properties

As a consequence of the formation of these *t4r* units, the 20-ring pores in ZEO-5 are no longer four-lobe shaped but are open through a rhomboid, saddle-shaped window with no protruding obstacles and with a much wider clearance (14.3 × 13.5 Å along the diagonals, 10.7 × 10.7 Å across opposite sides) (Fig. 2i). On the other hand, the 16-ring pores along directions normal to [001] are open through oblong 12.3 × 8.1 Å windows (Fig. 2j), more open than those in the precursors (Fig. 1b,c and Extended Data Fig. 2). Pore apertures of that size are unprecedented in stable silica zeolites. Despite its very open framework, ZEO-5 shows an outstanding stability that allows it to withstand calcination up to at least 1,000 °C and steaming under 10% H_2O up to at least 760 °C for 3 h (Extended Data Fig. 6), which is a consequence of the full connectivity and silica composition of its framework.

Condensation of ZEO-4A and ZEO-4B into ZEO-5 results, paradoxically for a 'condensation', in a notable expansion of the unit cell volume (12% and 7.6% expansion, respectively) (Supplementary Table 22), which is because of the longer size of the *t4r* unit compared with their precursors, *lau* or *d6r*, along the diagonals of the unit cell (Fig. 1), whereas the *c* parameter changes less than 0.5% as a result of the invariance of the basic ZEO-2 chain running along [001] (ref. 2). The new ZEO-5 zeolite holds the record for a low framework density silica polymorph at 11.07 Si atoms per 1 nm^3, well below the previous record holder ZEO-3 (ref. 2) (from which ZEO-5 is a *σ*-expansion) (Fig. 3), with framework density of 12.76 Si nm^{-3}. This translates into a calculated density of 1.10 g cm^{-3}, which is almost that of water. Furthermore, among all the zeolite framework types, irrespective of composition or stability, included in the Database of Zeolite Structures[10], only **RWY** has a lower framework density (7.6 T nm^{-3}). The **RWY** topology, containing 12-ring pores and very large cages, is not a zeolite oxide but is only realized in UCR-20, a sulfide of gallium and germanium with an extremely poor thermal stability[11]. Other frameworks listed in the database with rings equal to or larger than 18 rings and relatively low framework density of less than 15 Si nm^{-3} are all interrupted frameworks and/or have a germanosilicate or phosphate composition, with inherently poor stability (Supplementary Table 23). Because of its very open framework, ZEO-5 has unique textural properties (Fig. 2g, Supplementary Fig. 8 and Supplementary Table 24) compared with any reported zeolites. The Brunauer–Emmett–Teller surface areas of ZEO-5A and ZEO-5B reached record-breaking values of 1,533 and 1,832 m^2 g^{-1}, respectively, and the same is also true for their micropore volumes (0.40 or 0.38 cm^3 g^{-1}). This allows ZEO-5 to adsorb much more toluene than previously reported zeolites (Supplementary Fig. 9).

Introduction of heteroatoms and catalysis

We have introduced Ti atoms in ZEO-5 by a $TiCl_4$ vapour treatment (Methods) and compared the performance of the obtained Ti–ZEO-5 with that of Ti–Beta, the standard 3D large (12-ring) pore Ti–zeolite

catalyst, in the epoxidation of cyclooctene using both H_2O_2 and *tert*-butylhydroperoxide (TBHP) as oxidants. As shown in Extended Data Table 1, the cyclooctene conversion of both zeolites is similar when using the small H_2O_2, but ZEO-5 provides a slightly higher intrinsic activity of Ti (turnover number) because of a better cyclooctene diffusion (Supplementary Fig. 24). However, when the larger TBHP is used, the extra-large-pore Ti–ZEO-5 shows a much better performance than Ti–Beta because of the easier diffusion along extra-large pores. More importantly, Ti–ZEO-5 is a promising catalyst for the industrially relevant clean production of propylene oxide (PO) through the epoxidation of propylene with cumene hydroperoxide (CHP) as oxidant, the so-called CHP–PO process already commercialized by SumitomoChemical Co., Ltd. As shown in Extended Data Fig. 7 and Extended Data Table 2, conventional microporous 10-ring TS-1 and 12-ring Ti–Beta are almost inactive in this reaction. However, Ti–ZEO-5, because of its crystalline nature, its extra-large porosity similar to mesopores and its improved hydrothermal stability (Supplementary Fig. 25), demonstrates superiority to Ti–hexagonal mesoporous silica (Ti–HMS), the representative CHP–PO catalyst, in terms of site-time yield of propylene oxide.

Lattice energy of ZEO-5

As shown in Extended Data Fig. 8, the structure of ZEO-5 has a calculated lattice energy of 30 kJ mol^{-1} of Si relative to quartz, notably higher (approximately 8 kJ mol^{-1}) than those calculated for all other known zeolites and also notably larger than expected for its density (approximately 6 kJ mol^{-1}). We ascribe this high energy to the stress inherent to the *t4r* unit because it is known that even a *d4r* unit is much stressed for a pure silica composition[12]. ZEO-5 is actually at the edge of what Pophale et al.[13] consider 'feasible' (that is, thermodynamically accessible) zeolites. The realization of ZEO-5 emphasizes the idea that 'unfeasible' structures can in fact be reached through alternative synthesis routes[14,15].

Online content

Any methods, additional references, Nature Portfolio reporting summaries, source data, extended data, supplementary information, acknowledgements, peer review information; details of author contributions and competing interests; and statements of data and code availability are available at https://doi.org/10.1038/s41586-024-07194-6.

1. Lin, Q.-F. et al. A stable aluminosilicate zeolite with intersecting three-dimensional extra-large pores. *Science* **374**, 1605–1608 (2021).
2. Li, J. et al. A 3D extra-large-pore zeolite enabled by 1D-to-3D topotactic condensation of a chain silicate. *Science* **379**, 283–287 (2023).
3. Morris, R. E. Clicking zeolites together. *Science* **379**, 236–237 (2023).
4. Inagaki, S., Yokoi, T., Kubota, Y. & Tatsumi, T. Unique adsorption properties of organic–inorganic hybrid zeolite IEZ-1 with dimethylsilylene moieties. *Chem. Commun.* **48**, 5188–5190 (2007).
5. Fan, W., Wu, P., Namba, S. & Tatsumi, T. A titanosilicate that is structurally analogous to an MWW-type lamellar precursor. *Angew Chem. Int. Ed.* **43**, 236–240 (2004).
6. Smet, S. et al. Alternating copolymer of double four ring silicate and dimethyl silicone monomer–PSS-1. *Chem. Eur. J.* **23**, 11286–11293 (2017).
7. Xu, L. & Sun, J. Recent advances in the synthesis and application of two-dimensional zeolites. *Adv. Energy Mater.* **6**, 1600441 (2016).
8. Shamzhy, M., Gil, B., Opanasenko, M., Roth, W. J. & Čejka, J. MWW and MFI frameworks as model layered zeolites: structures, transformations, properties, and activity. *ACS Catal.* **11**, 2366–2396 (2021).
9. Dawson, D. M., Moran, R. F. & Ashbrook, S. E. An NMR crystallographic investigation of the relationships between the crystal structure and ^{29}Si isotropic chemical shift in silica zeolites. *J. Phys. Chem. C Nanomater. Interfaces* **121**, 15198–15210 (2017).
10. Baerlocher, C. & McCusker, L. B. *Database of Zeolite Structures* (Structure Commission of the International Zeolite Association, accessed 23 March 2023); http://www.iza-structure.org/databases/.
11. Zheng, N., Bu, X., Wang, B. & Feng, P. Microporous and photoluminescent chalcogenide zeolite analogs. *Science* **298**, 2366–2369 (2002).
12. Zicovich, C. M., Gándara, F., Monge, A. & Camblor, M. A. In situ transformation of TON silica zeolite into the less dense ITW: Structure-direction overcoming framework instability in the synthesis of SiO_2 zeolites. *J. Am. Chem. Soc.* **132**, 3461–3471 (2010).
13. Pophale, R., Cheeseman, P. A. & Deem, M. W. A database of new zeolite-like materials. *Phys. Chem. Chem. Phys.* **13**, 12407–12412 (2011).
14. Eliášová, P. et al. The ADOR mechanism for the synthesis of new zeolites. *Chem. Soc. Rev.* **44**, 7177–7206 (2015).
15. Mazur, M. et al. Synthesis of 'unfeasible' zeolites. *Nat. Chem.* **8**, 58–62 (2016).

Methods

Interchain expansion reactions

For the synthesis of ZEO-4A using DCDMS as silane reagent, 120 mg of one-dimensional zeolite chain precursor ZEO-2 (weight loss by thermogravimetric analysis around 68%, equal to 1.36 mmol SiO_2) (ref. 2 discusses the synthesis of ZEO-2) was added into 18 ml of 1.25 M HCl–EtOH solution (hydrogen chloride in ethanol solution; Merck) containing 164 µl of DCDMS (TCI; 1.36 mmol, 5.0 equivalents with respect to Si–OH groups) as the silane reagent. The suspension was stirred for few minutes and then transferred into a 30 ml Teflon vessel inserted in an autoclave. The autoclave was placed in an oven statically at 180 °C for 1 day to perform the interchain expansion posttreatment. After the reaction, the solid product and the acid solution were separated by filtration. The solid was finally washed with acetone (30 ml × 5) and dried to get the product ZEO-4A (91 mg; yield: 93% calculated by SiO_2). For the synthesis of ZEO-4B using TMCTS as silane reagent, 83 µl of TMCTS (TCI; 0.34 mmol, 5.0 equivalents) was used as the silane reagent, and similar steps were performed as mentioned to obtain the product ZEO-4B (94 mg; yield: 96%).

Calcination to form ZEO-5

To burn out the methyl groups and to allow the condensation of the newly introduced Si atoms, interchain-expanded zeolites ZEO-4 were calcined at 600 °C with a 3 h ramp and 6 h plateau to form the corresponding zeolites ZEO-5. Although the calcined materials all possess the same unique ZEO-5 structure, irrespective of the starting ZEO-4 material, to convincingly show, we will label them here as ZEO-5A or -5B depending on the precursor.

Structure solution and refinement from cRED

The structures of ZEO-4A, ZEO-4B and ZEO-5 were all solved ab initio by state-of-the-art cRED conducted on the needle-like crystals using a JEOL JEM-2100 transmission electron microscope (spherical aberration Cs: 1.0 mm, point resolution: 0.23 nm at 200 kV). The samples were prepared by first crushing the powder followed by dispersion in ethanol and ultrasonic treatment for 5 min. A drop of the dispersion was then deposited onto a 3-mm-wide copper transmission electron microscope grid covered by a carbon film. A high-tilt cryogenic sample holder equipped with temperature monitor (Gatan Company, Model 914) was used to freeze the sample to approximately 96 K to protect the crystallinity of the crystals. During the data collection, the goniometer was rotated continuously while the selected-area electron diffraction patterns were captured from the individual crystal simultaneously by a quad hybrid pixel detector QTPX-262k (512 × 512 pixels with the size of 55 µm; Amsterdam Sci. Ins.). Further details of the technique have been given elsewhere[16]. cRED datasets were used for the structure solution of ZEO-4A, ZEO-4B, ZEO-5A and ZEO-5B. The SHELX software package was used for structural analysis[17], where SHELXT was used for structure solution and SHELXL was used for structure refinement. Atomic scattering factors for electrons based on the neutral atoms were used.

Structure refinement using cRED, NPD and/or SPXRD datasets

SPXRD data were recorded in capillary mode at the Materials Science and Powder Diffraction beamline (bl04-MSPD) at the Spanish synchrotron radiation facility ALBA in Barcelona, Spain (λ = 0.61928 Å). NPD data were collected at the general purpose powder diffractometer of the China Spallation Neutron Source, Dongguan, China. The model refined using cRED data was used as the starting model for a Rietveld refinement against SPXRD data of ZEO-4A and ZEO-4B using Topas 6.1 (ref. 18). For ZEO-5, the final structure was refined by combining cRED, NPD and SPXRD without any restraints using Jana 2006 (ref. 19).

STEM

STEM measurements were performed using a spherical aberration (Cs)-corrected Titan X-FEG (field emission gun) FEI microscope equipped with a monochromator for the electron gun, a CEOS corrector for the electron probe and a Gatan Tridiem Energy Filter (GIF). Images were recorded using annular bright field and annular dark field detectors that were operated simultaneously. Samples were prepared by deeply crushing the powder using mortar and pestle; the powder was dispersed in ethanol, and a few drops of the suspension were placed onto holey carbon-coated copper microgrids. Multislice simulations were carried out using the QSTEM software[20], building the correspondent supercells for each material and introducing the same experimental parameters as used experimentally (being the spherical aberration 500 nm). The morphology of all materials was very similar, presenting a needle shape several micrometres long with very high crystallinity. Indeed, because of this particular morphology, obtaining information of the 20Rs pores (*c* axis) was extraordinarily difficult. Crystallites tend to lie along [110], in which the large pores as well as the small 4-, 5- and 6R units were clearly observed for ZEO-4A, ZEO-4B and ZEO-5 (Extended Data Fig. 5a–c, respectively). Despite the large similarities among the three structures under this view, subtle differences can be appreciated. Dashed yellow ellipses indicate the units that would be transformed upon calcination, *lau* and *d6r*, for ZEO-4A and ZEO-4B, respectively, into a connected triple four-ring *t4r*; the condensation brings about the expansion of the interchain spacing for ZEO-4A and ZEO-4B from 16.30 and 16.76 Å to 17.65 Å in ZEO-5. The simulated micrographs (in blue framed insets) perfectly match with the experimental data, corroborating the structure solution proposed. The formation of the 20R pores in ZEO-5 could be observed when the sample was tilted along [001] (Extended Data Fig. 5d). The atomic-resolution information reveals perfect connection of the three 4Rs (green dashed ellipsis) to form the large 20Rs rhomboid pores.

Catalysis

Ti has been introduced into ZEO-5 by a $TiCl_4$ gas-phase treatment. ZEO-5 (0.1 g) was activated at 573 K for 1 h in N_2 (43 ml min^{-1}). Then, another flow of N_2 (15 ml min^{-1}) was introduced into a bubbler containing $TiCl_4$ liquid at room temperature, carrying the $TiCl_4$ vapour to contact the zeolite powder, whereas the original N_2 flow was increased to 100 ml min^{-1}. The $TiCl_4$ treatment lasted for 5 min; then, the treated sample was further purged with pure N_2 gas for 1 h (43 ml min^{-1}). After cooling down, the sample was washed with distilled water, filtrated and dried at 393 K for 2 h, resulting in Ti–ZEO-5. The activity of Ti–ZEO-5 and Ti–Beta (as a standard 3D large-pore zeolite) in the epoxidation of cyclooctene was evaluated using both H_2O_2 (30% in water solution) and TBHP (5.5 M in decane) as oxidants. In both cases, 0.01 g catalyst was contacted with 1 mmol cyclooctene and 1 mmol oxidant, with 5 ml MeCN as solvent. The reaction was carried out at 333 K for 2 h. After removing the catalyst solid, the reaction mixture was analysed by gas chromatography (Shimadzu 2014, flame ionization detector) equipped with an Rtx-Wax capillary column. Cyclopentanone was used as an internal standard to quantify the amount of oxide product. The residual amount of H_2O_2 was determined by the titration method with 0.05 M $Ce(SO_4)_2$ aqueous solution. The activity of Ti–ZEO-5 was also evaluated in the epoxidation of propylene to propylene oxide with cumene hydroperoxide (80%; Alfa) by comparing with conventional TS-1, Ti–Beta and mesoporous Ti–HMS. The reactions were carried out in a 50 ml Teflon-lined high-pressure autoclave reactor. The titanosilicate catalyst (0.01 g), cumene hydroperoxide (10 mmol) and cumene solvent (10 ml; Sinopharm) were added in the reactor. The gas phase in autoclave was exchanged with propylene (99.9%; Shanghai Pujiang Special Gases) three times. Then, propylene (100 mmol) was charged into the autoclave by measuring the weight increase. The reactor was pressured to 2.4 MPa with nitrogen and then heated to 373 K in an oil

bath. The reaction was carried out under vigorous stirring at 373 K for 2 h. After removing the catalyst solid, the reaction mixture was analysed by gas chromatography (Shimadzu 2014, flame ionization detector) equipped with an Rtx-Wax capillary column. 2-Propanol was used as an internal standard to quantify the amount of propylene oxide product.

Calculations

Calculation methods are described in the Supplementary Information.

Data availability

The datasets generated and/or analysed during the current study have been deposited in DIGITAL.CSIC (https://doi.org/10.20350/digitalCSIC/16103). Crystallographic parameters for the structures of ZEO-4A, ZEO-4B and ZEO-5 refined against synchrotron powder X-ray diffraction data (SPXRD) and continuous rotation electron diffraction (cRED) data are archived at the Cambridge Crystallographic Data Center (www.ccdc.cam.ac.uk/) under reference numbers 2249198 and 2249199 (ZEO-4A and ZEO-4B, SPXRD), 2249103–2249106 (ZEO-5A, ZEO-5B, ZEO-4A and ZEO-4B, cRED) and 2288122 (ZEO-5, combining cRED, SPXRD and neutron powder diffraction). Source data are provided with this paper.

16. Li, J., Lin, C., Ma, T. & Sun, J. Atomic-resolution structures from polycrystalline covalent organic frameworks with enhanced cryo-cRED. *Nat. Commun.* **13**, 4016 (2022).
17. Sheldrick, G. M. Phase annealing in SHELX-90: direct methods for larger structures. *Acta Cryst.* **A46**, 467–473 (1990).
18. Coelho, A. A. TOPAS and TOPAS-Academic: an optimization program integrating computer algebra and crystallographic objects written in C++. *J. Appl. Cryst.* **51**, 210–218 (2018).
19. Petricek, V., Dusek, M. & Palatinus, L. Crystallographic computing system JANA2006: general features. *Z. Kristallogr.* **229**, 345–352 (2014).
20. Koch, C. T. *Determination of Core Structure Periodicity and Point Defect Density Along Dislocations*. PhD thesis, Arizona State Univ. (2002).
21. Deem, M. W., Pophale, R., Cheeseman, P. A. & Earl, D. J. Computational discovery of new zeolite-like materials. *J. Phys. Chem. C* **113**, 21353–21360 (2009).

Acknowledgements Financial support from the Spanish Ministry of Science Innovation (PID2019-105479RB-I00 and TED2021-131223B-I00 Projects, MCIN/AEI/10.13039/501100011033 and grants RYC2018-024561-I and FJC2018-035697-I); the National Natural Science Foundation of China (grants 22371121, 22288101, 21920102005, 21835002, 22271115 and 52270111); the National Key Research and Development Program of China (grants 2022YFA1503600, 2021YFA1501202 and 2021YFA1501401); the 111 Project (grant B17020); the Fundamental Research Funds for the Central Universities of China (grant 020514380306); and the Consejería de Universidades, Investigación e Innovación, Junta de Andalucía (grant POSTDOC_21_00069) is gratefully acknowledged. Continuous rotation electron diffraction data were collected at the Electron Microscopy Center, Department of Materials and Environmental Chemistry at Stockholm University with the support of the Knut and Alice Wallenberg Foundation (grant 2012-0112) through the 3DEM-NATUR Project. We acknowledge the use of instrumentation provided by the National Facility ELECMI (Integrated Infrastructure for Electron Microscopy of Materials) ICTS (Instalación Científico Técnica Singular) node Laboratorio de Microscopías Avanzadas at the University of Zaragoza. Additional funding from the European Union's Horizon 2020 Research and Innovation Program (grant 823717-ESTEEM3) and the Regional Government of Aragon (grant DGA E13_20R) is also acknowledged. H.Y. is grateful to the China Scholarship Council for a PhD grant. Synchrotron powder X-ray diffraction data experiments were performed at the MSPD (Materials Science Powder Diffraction) beamline bl04 at the ALBA Spanish Synchrotron with the collaboration of the ALBA staff. We thank C3UPO (Centro de Cálculo Científico de la Universidad Pablo de Olavide) for providing high-performance computing facilities and L.-H. He for help with the powder neutron diffractions data collection performed at the general purpose powder diffractometer of China Spallation Neutron Source, Dongguan, China (Project General Purpose Powder Diffractometer, P1823060200002).

Author contributions M.A.C. conceived the project. J.L., P.W., J.Y. and M.A.C. supervised this work. Z.R.G., H.Y., F.-J.C. and Zijian Niu performed the synthesis. C.M. and J.L. solved the structures, and J.H. and J.L. performed Rietveld refinement. A.M. performed the Cs-corrected STEM analysis. Z.R.G. analysed the topology. S.R.G.B. performed and analysed all computer calculations. Z.R.G., H.Y., F.-J.C., Zijian Niu, Ziwen Niu, H.D., C.M.-Á., H.X., W.F. and M.A.C. carried out the physicochemical characterization. S.X., Y.Z. and J.X. performed two-dimensional and dynamic nuclear polarization magic-angle spinning nuclear magnetic resonance spectroscopy. H.D. and H.H. worked on the volatile organic compounds adsorption. Ziwen Niu, X.L., H.X. and P.W. performed the catalytic tests. M.A.C. wrote the initial draft of the manuscript. J.L., P.W., J.Y. and M.A.C. organized the work and the draft. All the authors discussed the results and revised the manuscript.

Competing interests The authors declare no competing interests.

Additional information

Supplementary information The online version contains supplementary material available at https://doi.org/10.1038/s41586-024-07194-6.

Correspondence and requests for materials should be addressed to Jian Li, Peng Wu, Jihong Yu or Miguel A. Camblor.

Peer review information *Nature* thanks Alex Yip and the other, anonymous, reviewer(s) for their contribution to the peer review of this work. Peer reviewer reports are available.

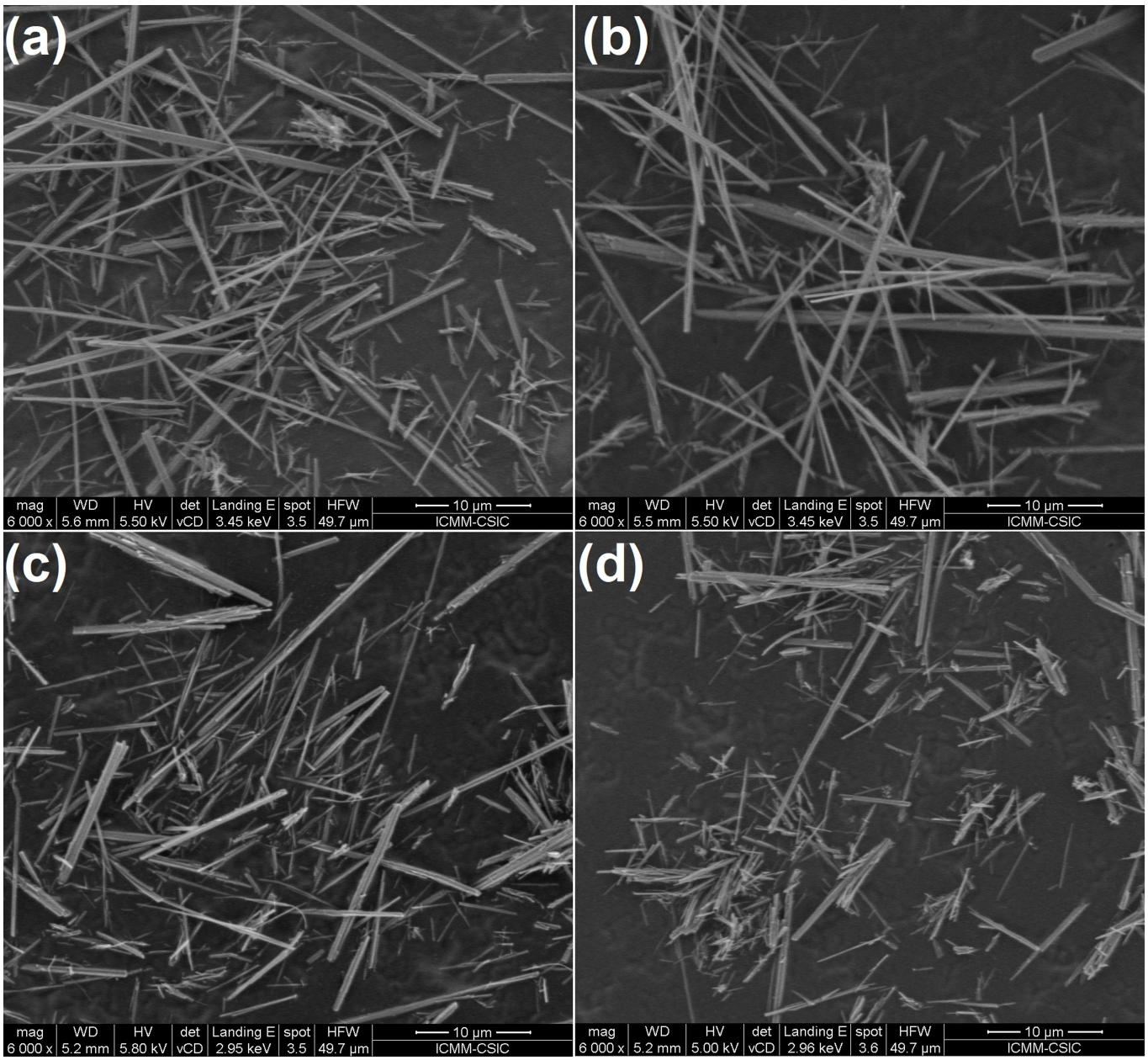

Extended Data Fig. 1 | Field emission scanning electron microscopy. FESEM images of ZEO-4A (a), ZEO-4B (b), ZEO-5A (c), and ZEO-5B (d), showing the same morphology of ZEO-2[2].

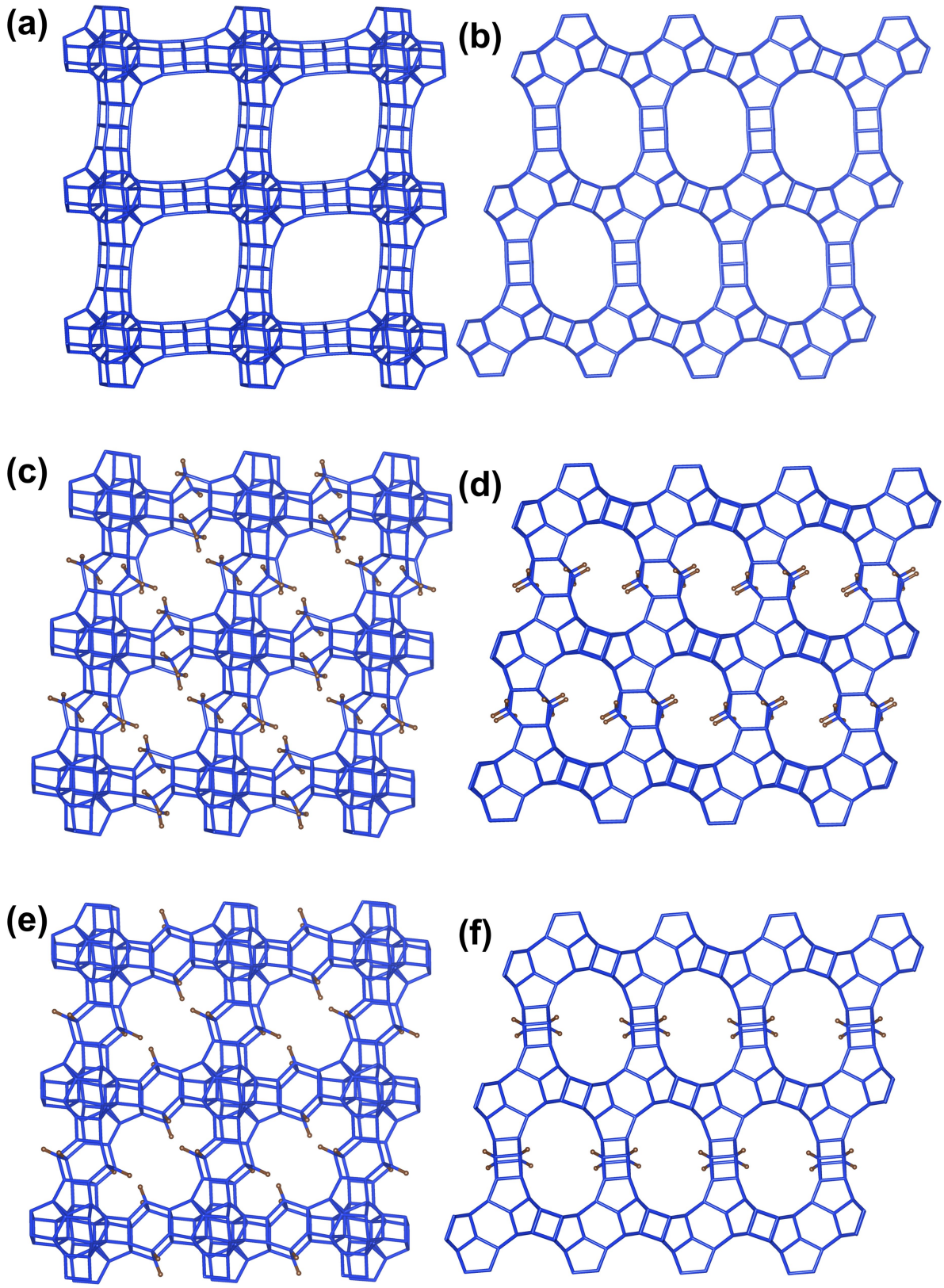

Extended Data Fig. 2 | Zeolite porosity. The pores in fully connected framework ZEO-5 (a-b) and interrupted structure ZEO-4A (c-d) and ZEO-4B (e-f), the 20-ring pore (a, c, e) approximately along [001] and the 16-ring pore (b, d, f) approximately along [110].

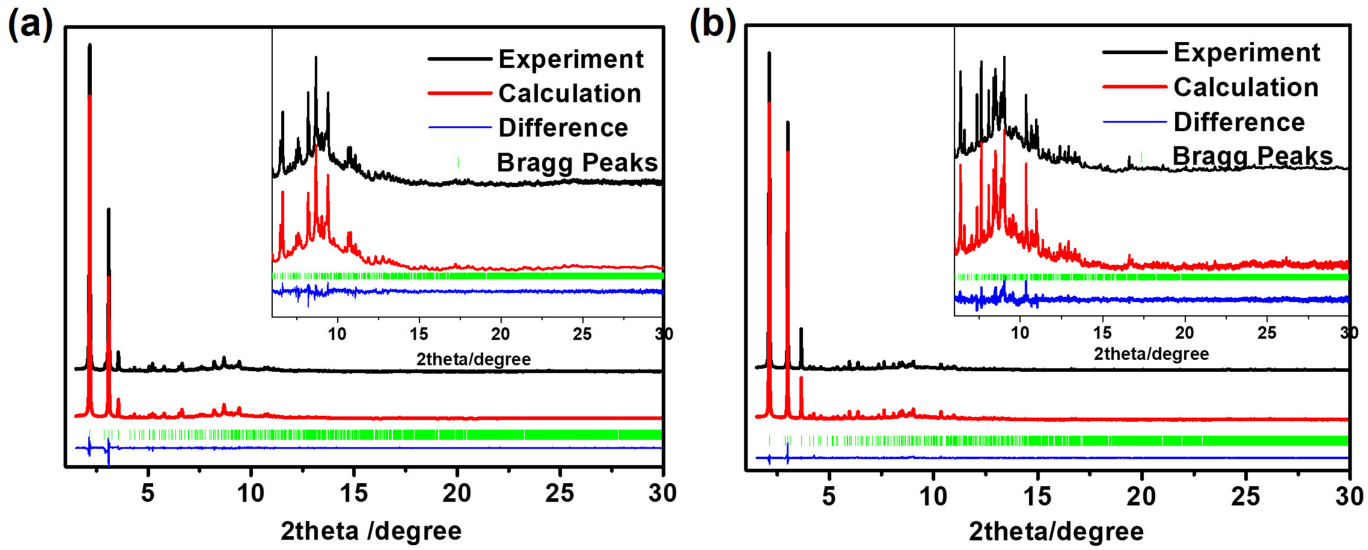

Extended Data Fig. 3 | Rietveld structure refinement. Rietveld refinement plots of (a) ZEO-4A and (b) ZEO-4B against SPXRD (λ = 0.61928 Å).

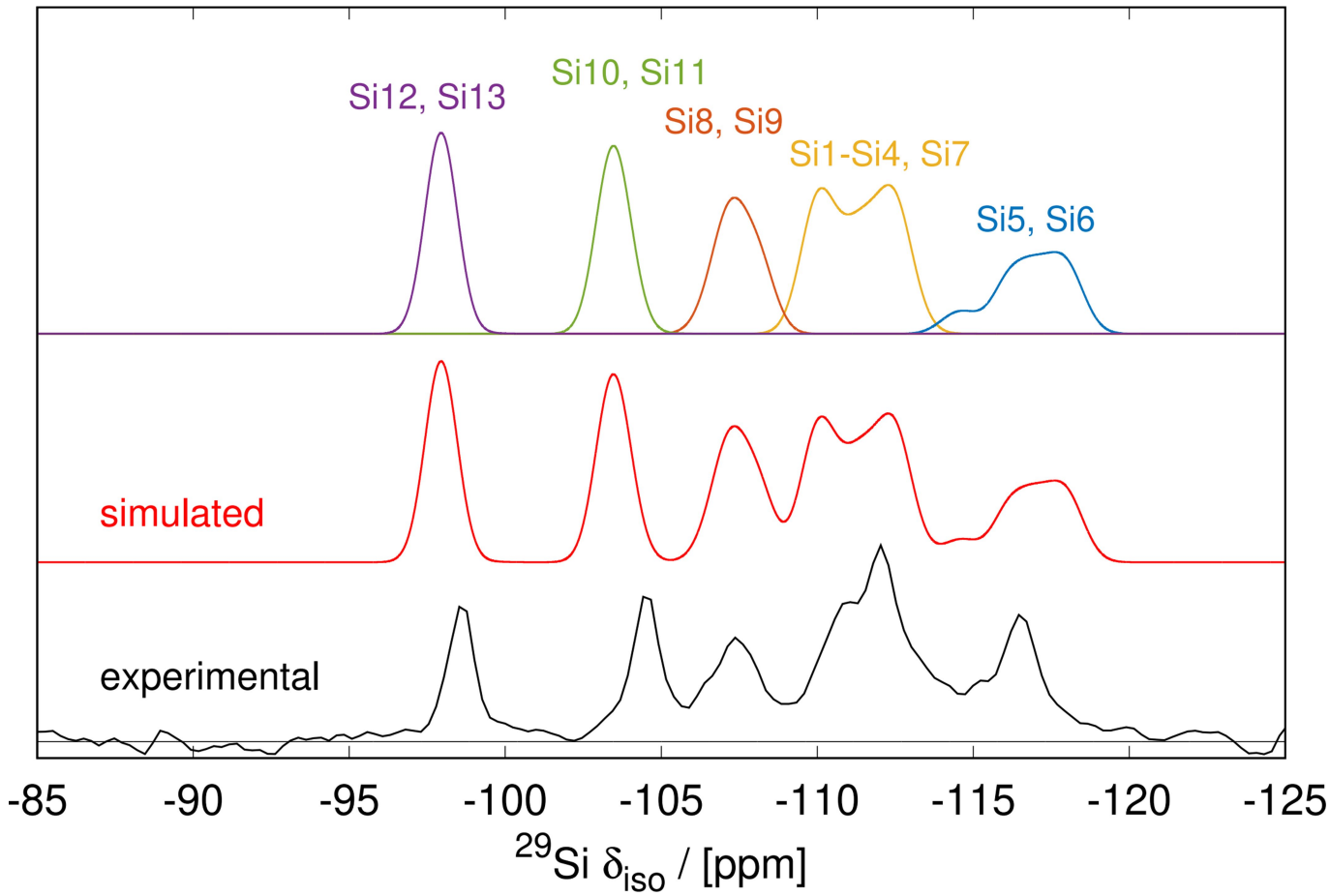

Extended Data Fig. 4 | ^{29}Si MAS NMR spectroscopy. ^{29}Si MAS NMR spectra of ZEO-5 (from bottom): Experimental, DFT-simulated and individual components (see SM). The DFT study confirms that the very low field signal at −98 ppm corresponds to the Si sites in the central 4-ring of the *t*4*r* unit (Si12 and Si13).

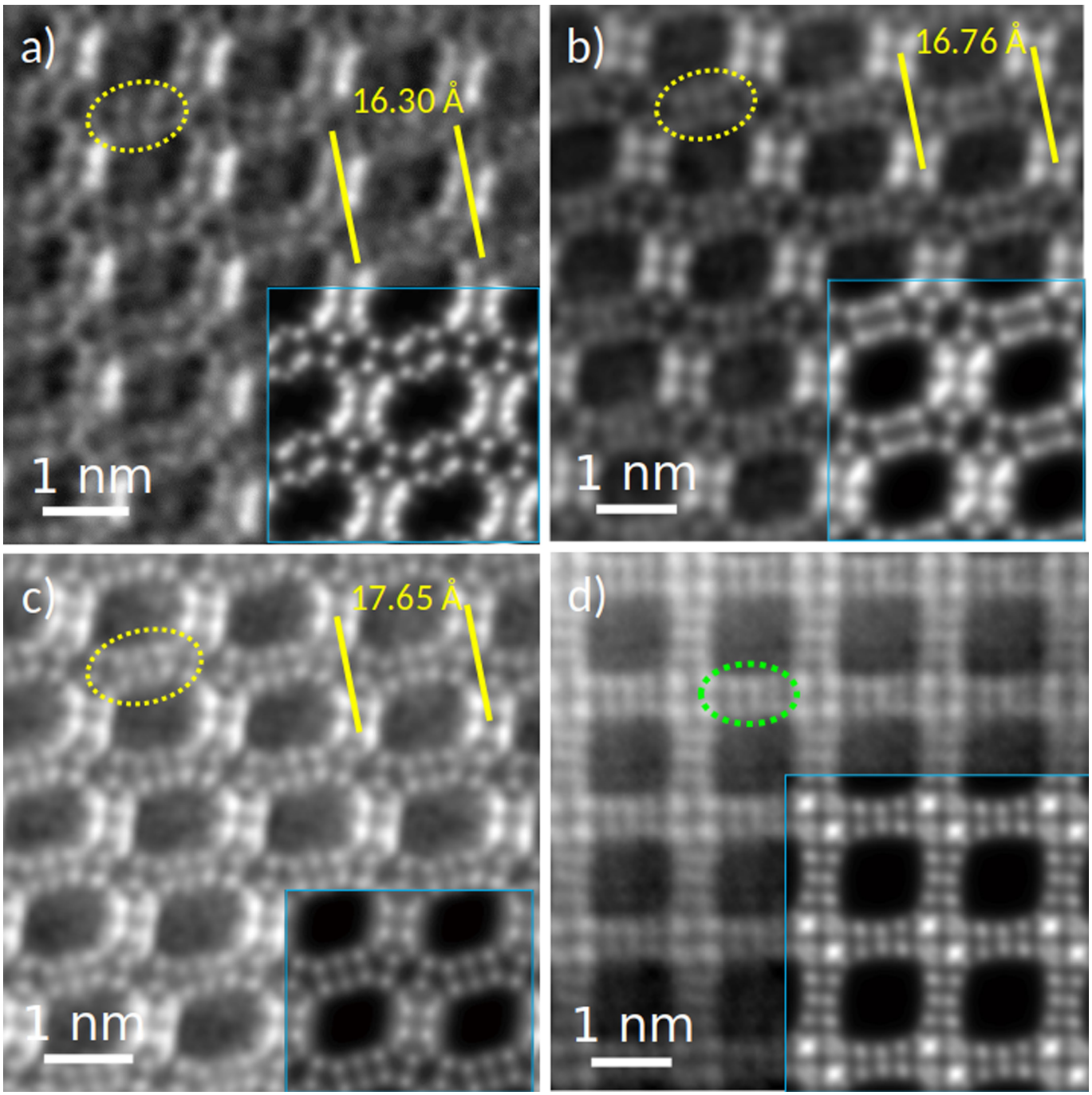

Extended Data Fig. 5 | Cs-corrected STEM analysis of the pore systems. Along [110] (a-c) for a) ZEO-4A b) ZEO-4B and c) ZEO-5 with the units involved in the structural transformation circumscribed by yellow dashed ellipses. Condensation of ZEO-4A and ZEO-4B into ZEO-5 brings about an expansion of the interchain distance, as shown by the yellow solid lines and in full agreement with the refined structures. In d) the 20 R pore of ZEO-5 is observed along the [001] projection. A *t4r* unit is marked by a green dashed ellipse. The micrographs simulated using the Rietveld refined data are shown in the insets and corroborate the structural models.

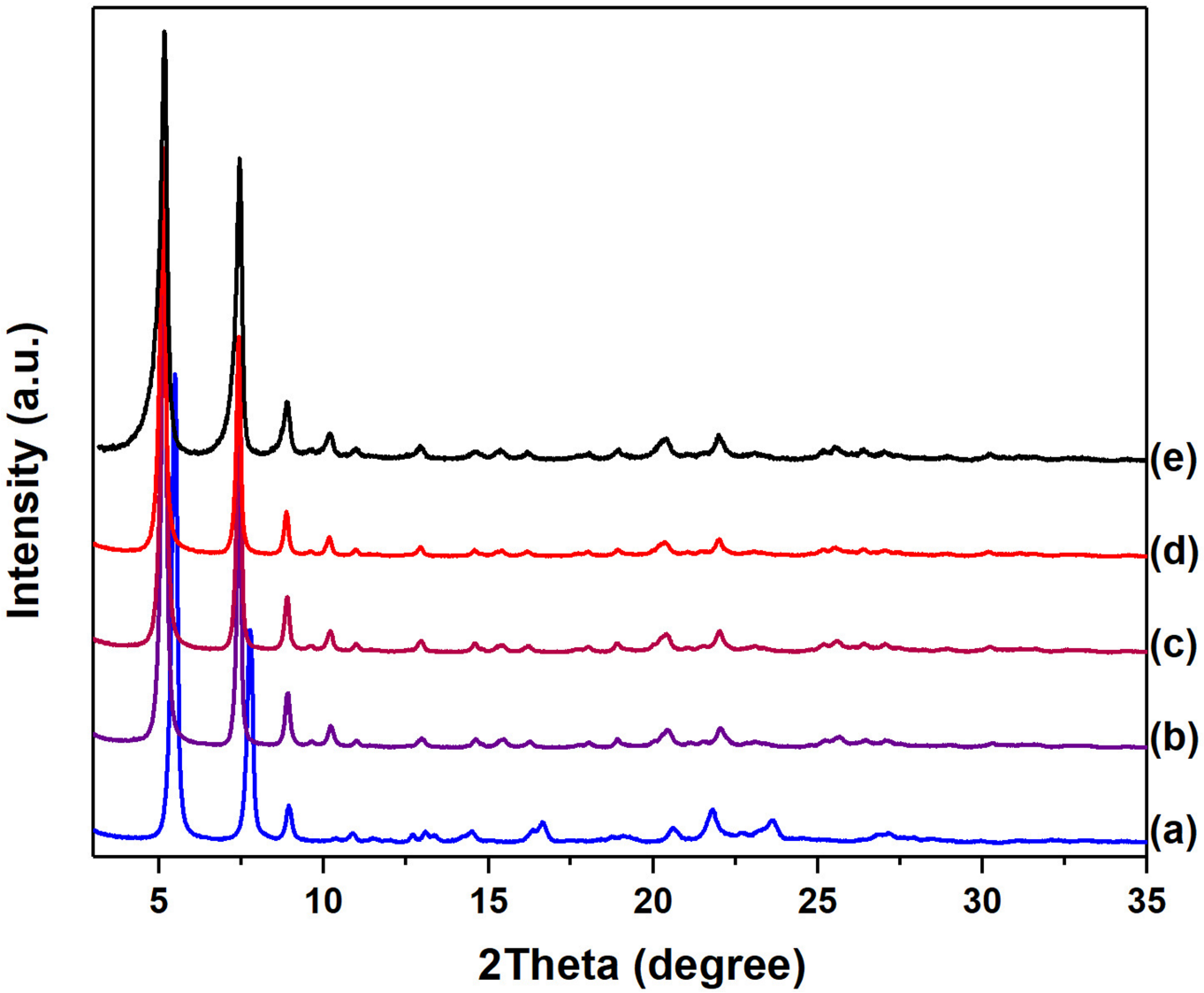

Extended Data Fig. 6 | Thermal and hydrothermal stability tests for ZEO-5. PXRD patterns of ZEO-4A (a), and ZEO-5 upon calcination at 600 °C (b), 800 °C (c), and 1000 °C (d) with one-hour plateau, and ZEO-5 steamed at 760 °C for 3 h under 10% H_2O (e).

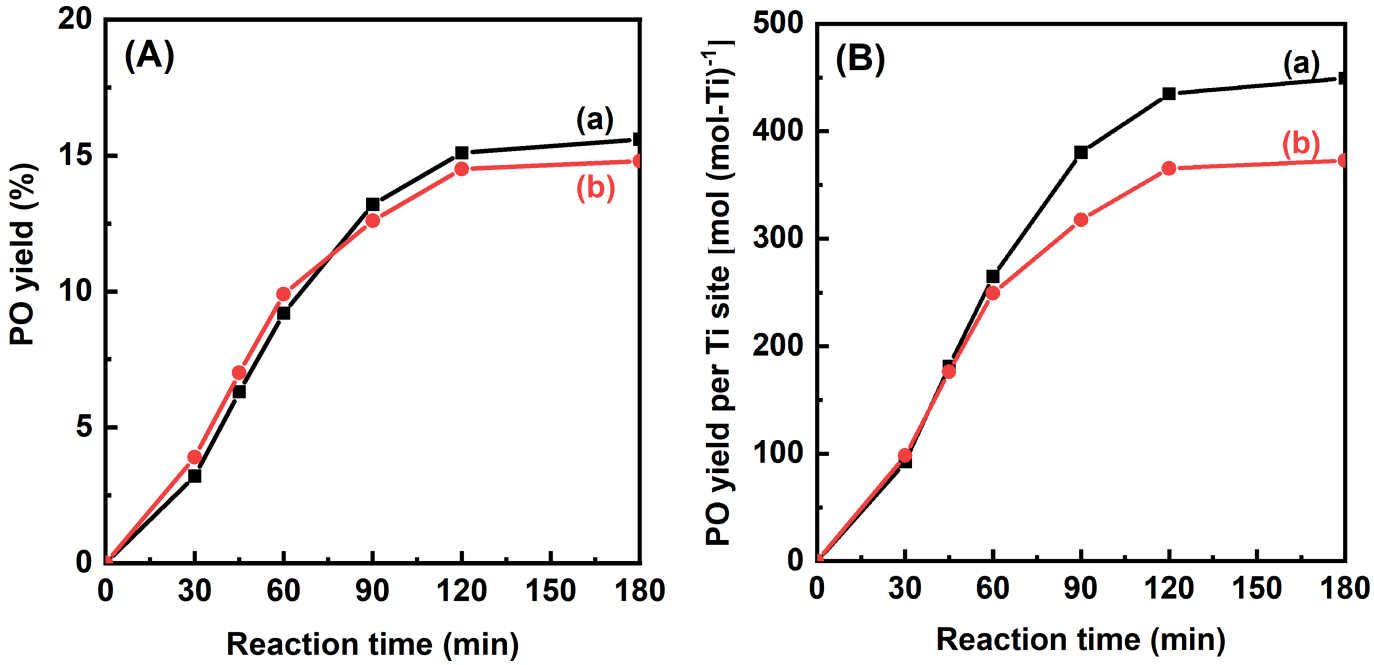

Extended Data Fig. 7 | Catalytic oxidation of propylene. Dependence of PO yield (A) and specific PO yield per Ti site (B) on reaction time over Ti-ZEO-5 (a) and Ti-HMS (b) catalysts in the propylene epoxidation reaction. Reaction conditions: catalyst, 0.01 g; cumene hydroperoxide (CHP), 10 mmol; propylene, 100 mmol; cumene solvent, 10 mL; temp., 373 K; reaction pressure, 2.4 MPa.

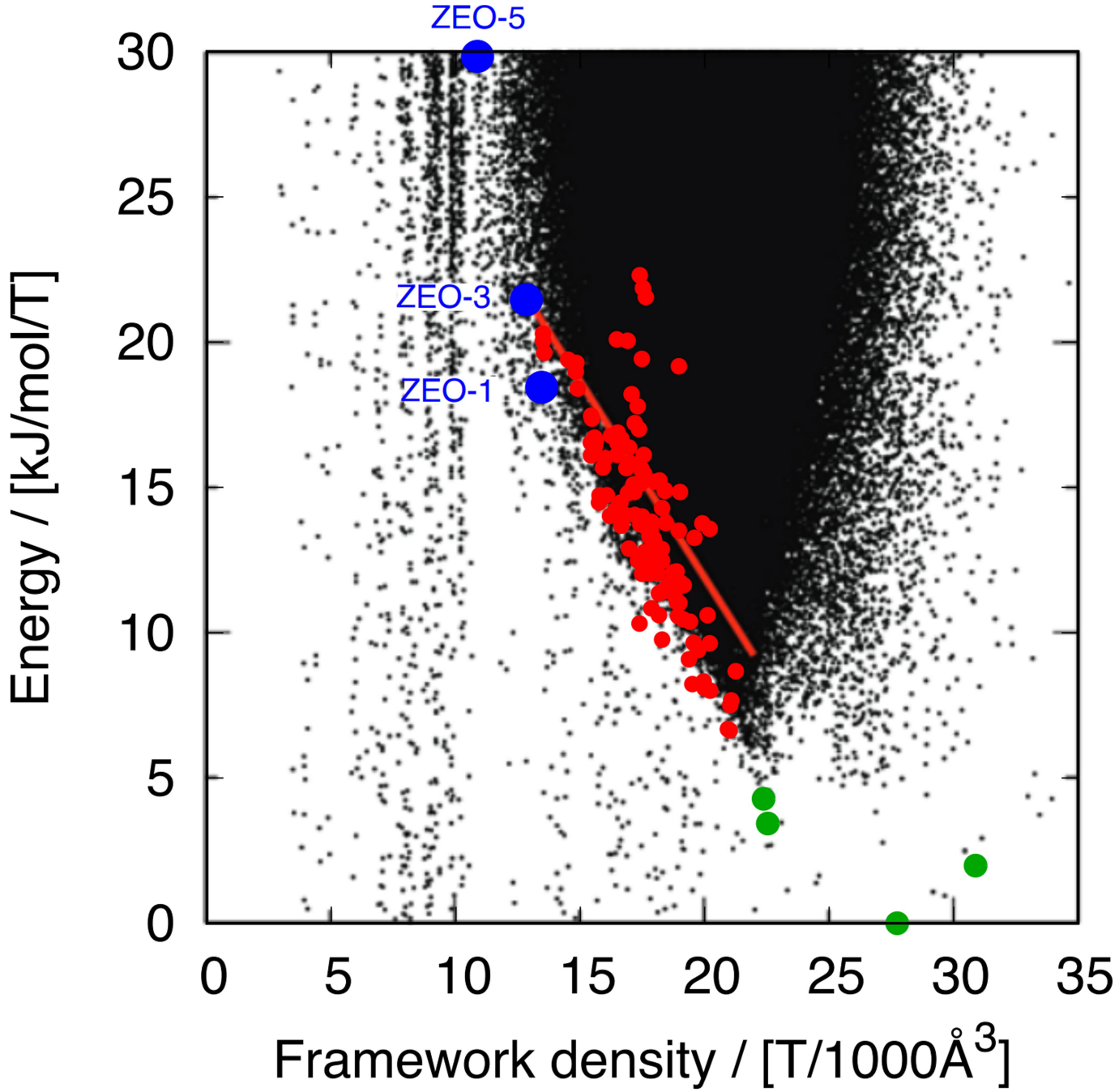

Extended Data Fig. 8 | Framework density – Energy plot. The lattice energy versus density of the zeolite-like materials (black dots) was minimized using the Sanders-Leslie-Catlow (SLC) interatomic potential, according to Deem et al.[21] The red line appears in the original publication as "the linear fit of energy versus density for the known zeolite structures." We have included our data points for updated porous crystalline silica polymorphs from the IZA database (red points), dense silica polymorphs (green points), and ZEO-1, ZEO-3, and ZEO-5 materials (large blue points) calculated using the same methodology. Reprinted (adapted) with permission from ref. 21, copyright 2009 American Chemical Society.

Extended Data Table 1 | A comparison of cyclooctene oxidation between Ti-ZEO-5 and Ti-Beta[a]

Catalyst/oxidant	Si/Ti [b]	Cyclooctene (%)		TON [c]
		conv.	oxide sel.	
Ti-ZEO-5/H_2O_2	48	8.8	99.8	25
Ti-ZEO-5/TBHP	48	14.7	99.9	44
Ti-Beta/H_2O_2	44	6.2	99.8	18
Ti-Beta/TBHP	44	3.5	99.9	10

Remarks:
[a] Reaction conditions: catalyst, 0.01 g; cyclooctene, 1 mmol; H_2O_2 (30 wt.%) or tert-butyl hydroperoxide (5.5 M in decane), 1 mmol; MeCN solvent, 5 mL; temp., 333 K; time, 2 h.
[b] Given by ICP analysis.
[c] Turnover number in mol (mol-Ti)$^{-1}$.

Extended Data Table 2 | A comparison of propylene oxidation with cumene hydroperoxide between Ti-ZEO-5 and other titanosilicates[a]

Catalysts	Pore structure	Si/Ti [b]	PO yield [c] (%)	STY [d] (h^{-1})
Ti-ZEO-5	3D 20×16×16-ring	48	15.1	217
Ti-HMS	mesopore	42	14.5	183
Ti-Beta	3D 12-ring	44	0.8	10.5
TS-1	3D 10-ring	40	0.2	2.4

Remarks:

[a] Reaction conditions: catalyst, 0.01 g; cumene hydroperoxide (CHP), 10 mmol; propylene, 100 mmol; cumene solvent, 10 mL; temp., 373 K; time, 2 h; reaction pressure, 2.4 MPa.

[b] Given by ICP analysis.

[c] PO selectivity >99% in all cases.

[d] Site-time-yield (STY), moles of PO product per mol of Ti per hour.